Tailoring of keV-Ion Beams by Image Charge when Transmitting through Rhombic and Rectangular Shaped Nanocapillaries

H.-Q. Zhang,[1,*] N. Akram,[1] P. Skog,[1] I. L. Soroka,[1,†] C. Trautmann,[2] and R. Schuch[1,‡]

[1]*Physics Department, Stockholm University, S-106 91 Stockholm, Sweden*

[2]*GSI Helmholtzzentrum für Schwerionenforschung, D-64291 Darmstadt, Germany*

(Received 18 October 2011; published 7 May 2012)

We report on an unexpected effect of tailoring transmission profiles of Ne^{7+} ions through nanocapillaries of rhombic and rectangular cross sections in mica. We find that capillaries of rhombic cross sections produce rectangular shaped ion transmission profiles and, vice versa, that capillaries of rectangular geometry give a rhombic beam shape. This shaping effect only occurs for transmitted ions and is absent for the small fraction of neutralized particles. The experimental findings and simulations of the projectile trajectories give clear evidence that the observed effect is due to the image forces experienced by the transmitting ions. This novel beam shaping mechanism suggests applications for the guiding, focusing, and shaping of ion beams.

DOI: 10.1103/PhysRevLett.108.193202 PACS numbers: 34.50.−s, 61.85.+p, 79.20.Rf, 81.07.De

Membranes with nanosized capillaries have found ample applications in a large variety of areas, including physics, chemistry, biology, or material science [1]. They are used as filters for biological molecules [2,3] and biodetection arrays [4]. Transport phenomena of charges in nanoelectronics are being considered [5], and nanocapillaries are used as gated filters [6–8] or as sensors to transport or identify charged particles [9,10].

A recent study showed a new phenomenon when transmitting ions through nanocapillaries in polymeric membranes [11]. It revealed the possibility of ion transport through insulating channels at angles much larger than the angle allowed by their aspect ratio. The transmission occurs without energy loss and charge exchange, which is of great interest for new ion-beam optics. The phenomenon is explained by the deposition of charges on the insulating capillary walls due to initial ion impact. Subsequent ions are then guided through the capillaries, in a manner similar to the channeling of particles in a crystal lattice potential [12], with the difference that, in ion guiding, the guiding potential is self-arranged and mesoscopic. Close collisions are avoided, and there is no significant energy loss or charge exchange in ion guiding. Ions follow along the capillary and exit parallel to the channel orientation, independent of their entrance angles. This is very effective with slow highly charged ions (HCI) and has been observed for various insulating membranes, such as *polyethylene terephthalate* (PET) [11,13–15], SiO_2 [16–18], and Al_2O_3 [19–21], containing millions of nanocapillaries with size varying from several tens to hundreds of nanometers. Even single tapered glass capillaries have been used to produce micrometer sized ion beams [9,10] and applied to selectively irradiate individual constituents of biological cells [22].

The guiding of ions through insulating capillaries requires a charging up of the walls, and thus it is a time-dependent process. Maximum transmission is achieved after the charge deposition from incident ions and the draining through various discharge channels have reached a state of equilibrium [11,23]. It has been shown that a small number of charge patches is sequentially formed in the charging-up process [14,15,17,18] that guides ions in the stationary state of transmission. All the studies, so far, were done with circular capillaries, having complete rotational symmetry.

In contrast to the previous experiments on the guiding of HCI, we have utilized nanocapillaries of noncircular cross sections. We report here ion transport through insulating nanocapillaries of rhombic and rectangular shapes. Surprisingly, we found that the ion-beam profiles are tailored in an intriguing way by the geometrical shape of the nanocapillaries. Capillaries of rhombic cross sections produce rectangular shaped ion transmission profiles, and, vice versa, capillaries of rectangular geometry give a rhombic beam shape. It is shown that the beam shaping is mediated by the image charge induced when the projectiles transmit through the nanochannels.

Membranes with nanocapillaries were fabricated by exposing 20-μm-thick muscovite and 10-μm-thick phlogopite mica wafers to 2.3-GeV Pb and 1.4-GeV Xe ions, respectively. The irradiation was performed at the linear accelerator UNILAC of the GSI Helmholtz Centre under normal beam incidence, applying a fluence of 5×10^7 ions/cm^2. Given by their large mass and high energy, the projectiles pass through the entire thickness of the samples and produce tracks of few nanometers in diameter [24]. The irradiated samples were then etched at room temperature in a 20% aqueous solution of hydrofluoric acid, the muscovite for 10 minutes and the phlogopite mica for 3 minutes. Each ion track is preferentially attacked at a higher rate than the undamaged surrounding matrix material, leading to highly parallel oriented nanocapillaries. In contrast to round shaped channels in

isotropic polymers [11,13–15], the cross section in mica is determined by crystal orientation-dependent etching rates. As shown by scanning electron microscopy (SEM), this leads to a rhombic cross section in muscovite mica and a rectangular cross section in phlogopite mica, with the axes of all nanocapillaries being aligned along the same orientation [Figs. 1(a) and 1(b)].

The rhombic channels in muscovite mica have acute angles of 60° and obtuse angles of 120°, with a long axis of 248 nm and a short axis of 142 nm, and the channel length of 20 μm gives the geometrical opening angle of 0.4° for the short axis. The area density (determined by the applied ion fluence) together with the cross section of the capillaries yield a geometrical transparency (porosity) of 0.9%, which is sufficiently low to regard the nanochannels as individual well-separated nonoverlapping objects. In phlogopite mica, track etching resulted in rectangular shaped capillaries. This is in contrast to earlier findings of triangular cross sections described in Ref. [25], probably due to crystal orientation effects. The nearly perfect rectangular capillaries have dimensions of 450 nm by 215 nm, corresponding to a porosity of 4.8%. The membrane thickness of 10 μm results in a geometrical opening angle of 1.23° along the short sides. To avoid macroscopic charge-up, Au films of 10 nm thickness were evaporated on both of the membrane surfaces.

The transmission experiments with HCI were performed at the ECR ion source and S-EBIT of Stockholm University. Beams of 7-keV Ne^{7+} ions were collimated to a divergence of less than 0.2°, a size of 2×2 mm^2, and an intensity of 8 to 80 pA/mm^2 at the membrane position by a pair of four-jaw slits, set 1.55 m apart. The capillary membrane was mounted on a goniometer, allowing independent adjustment in three spatial directions and around two rotational axes. The transmitted ions were imaged using microchannel plates with a resistive anode [17,18]. Downstream of the capillary membrane, an electrostatic deflector allowed the analysis of the charge states of the transmitted ions [Fig. 1(c)]. The capillaries can be oriented in the direction of the incident beam by the tilt angle α. The observation angles ϕ and θ, related to the hit position in the detection plane, are given with respect to the incident beam direction [see Fig. 1(c)].

The primary beam profile and angular distributions of the ions transmitted through the rhombic and rectangular capillaries, with a tilt angle $\alpha = 0° \pm 0.25°$, are shown in Fig. 2. The incident beam profile is imaged by the 2D detector in the same way as described in Ref. [18]. We find that transmission through the rectangular capillaries leads to a rhombic angular distribution, with the long axis

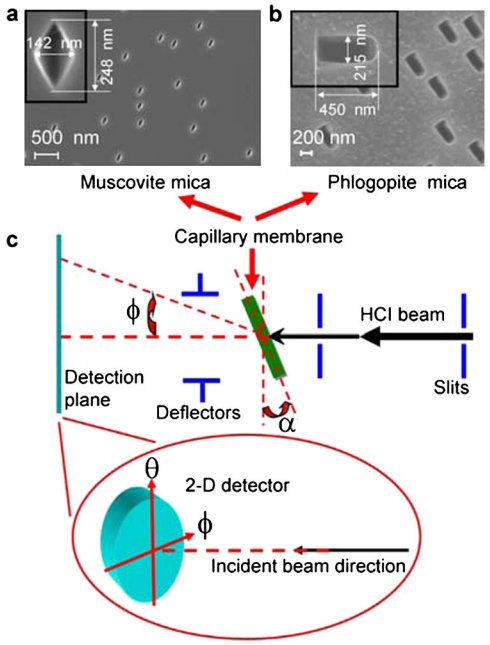

FIG. 1 (color online). SEM images of track-etched mica membranes with nanocapillaries of (a) rhombic and (b) rectangular cross sections and (c) a schematic view of the setup for the ion transmission experiments.

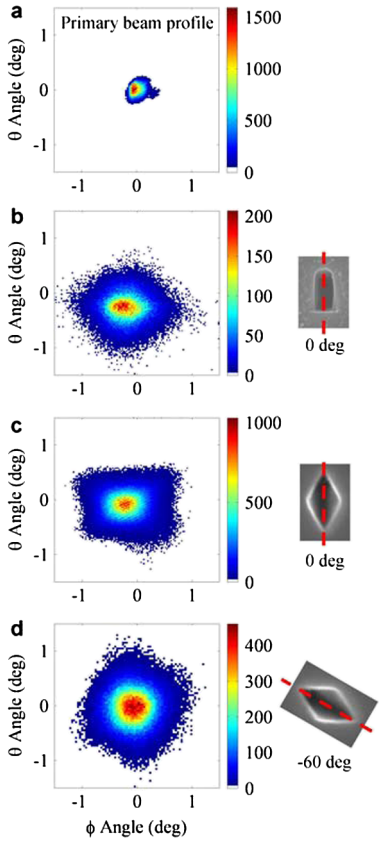

FIG. 2 (color online). (a) Primary beam profile and two-dimensional angular distributions for 7-keV Ne^{7+} transmitted through mica capillaries of (b) rectangular and (c),(d) rhombic cross sections with the corresponding orientations of the long sides of the rectangles and the long axes of the rhombi in a plane perpendicular to the beam (as indicated on the right panel).

of the rhombus parallel to the short sides of the rectangles [Fig. 2(b)]. In contrast, rhombic capillaries tailor the transmission profile into a rectangular distribution, with the long side aligned along the short axes of the rhombi [Fig. 2(c)]. Obviously, the transmission profile and the shape of the cross section of the capillaries are complementary to each other. We also measured the transmitted profiles for various orientations of the long axes of the rhombi and found that the profile rotates accordingly [Fig. 2(d)], giving strong evidence that the angular distribution does not originate from the shape of the primary beam [Fig. 2(a)].

When applying a voltage to the deflector placed between the capillary membrane and the detector, we find that more than 90% of the transmitted particles are the initial Ne^{7+} ions, showing a rectangular shape for the nanocapillaries of rhombic cross sections, as seen in Fig. 3. There is a weak component of the beam ($\sim 9\%$) that remains unshifted. This weak component is ascribed to neutral projectiles, producing an angular distribution which seems to image the rhombic shape of the capillaries as a shadow on the detector [Fig. 3(b)].

Obviously, only the ionic portion of the transmitted beam is tailored by the interaction with the capillary wall. We considered two forces involved: (1) due to the directly deposited charge on the walls and (2) due to the image charge induced by the ions when they are passing through the capillaries. In order to identify the role of these forces in tailoring the transmitted profiles, we started our measurements with uncharged capillaries. Then, we measured the time evolution of the angular distribution of the transmitted beam near zero tilt angle ($\alpha = -0.25°$ for rhombic and $\alpha = +0.4°$ for rectangular capillaries). We recorded the angular distributions at the very early stage of transmission when the walls of the nanocapillaries are not yet sufficiently charged for case (1). In case (2), the interaction between the ions and walls is expected to be instantaneous. Figure 4 shows images after a few ions (in averages 4 and 21 for rhombic and rectangular cross sections, respectively) have entered a single capillary. This number of incident ions is much less than required for generating the guiding charge patches on the capillary walls [17]. The characteristic shapes appearing for such a low number of ions [Figs. 4(a) and 4(c)] give evidence that the ion transmission profile is tailored by the image forces (2) rather than by Coulomb forces from the deposited charge (1). We also investigated the interplay of the deposited charge and the image charge by varying tilt angles [26,27]. At tilt angles larger than the geometrically allowed angle, the angular distributions are getting distorted from the rectangles. While close to the tilt angle zero, the transmitted angular distributions are rectangles after the stationary state of the transmission. Whether the image force is screened by the deposited charge depends on the locality of the deposited charge and thus the surface density of the deposited charge. For small tilt angles close to zero, the deposited charge is rather evenly distributed, while, at tilt angles larger than the geometrically allowed angle, the deposited charges are more localized and thus affect the image charge more.

We simulated the angular distributions of the transmitted ions by considering the image forces [Figs. 4(b) and 4(d)].

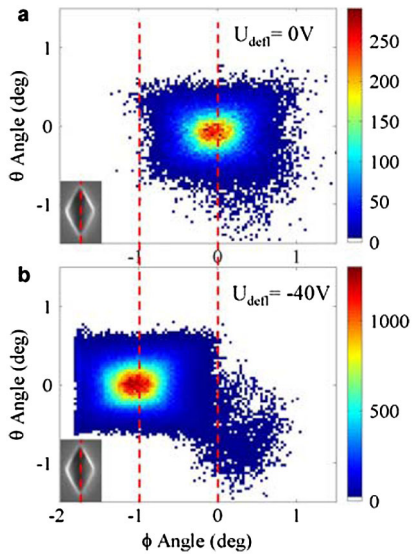

FIG. 3 (color online). Images of ions transmitted at tilt angle 0° through rhombic nanocapillaries (the cross section with the orientation of the rhombi is shown in the lower-left-hand corners) (a) without and (b) with applying an electric deflection field.

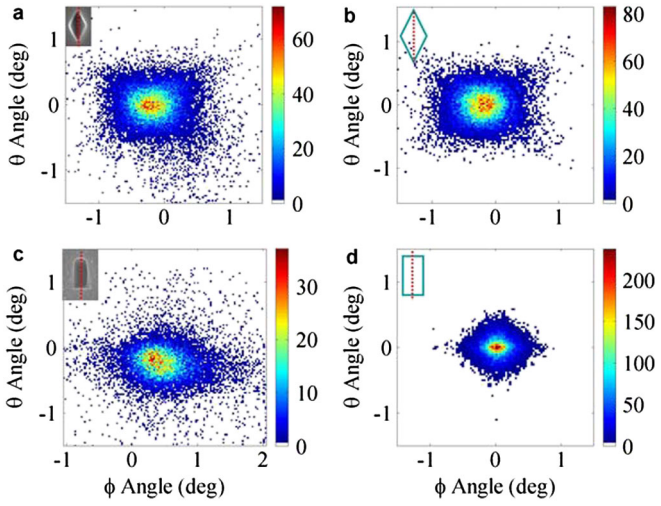

FIG. 4 (color online). Initial angular distributions of the transmitted ions are shown: experimental profiles with $\alpha = -0.25°$ in (a) and with $\alpha = +0.4°$ in (c) and simulated transmission profiles considering the image force effect for rhombic capillaries in (b) and rectangular capillaries in (d), respectively. The insets in the upper-left-hand corners of each graph show the orientations of the rhombi and rectangles.

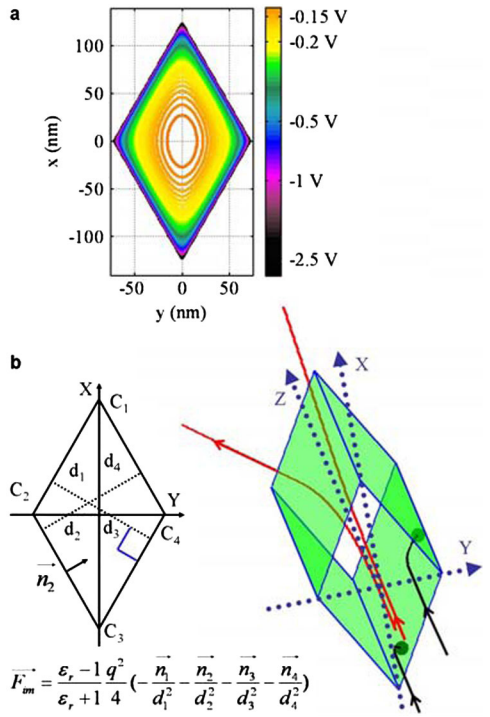

FIG. 5 (color online). The equipotential lines of the image force for a charge in a rhombus are shown in (a), and, in (b), the image force superposition and the ion trajectories are shown, where ε_r is the relative dielectric constant and q is the charge state of the ion (note that the aspect ratio of the capillary is strongly reduced to show the ion trajectories).

The net force on the projectile is taken into account in the first order by superposition of the image forces from each of the nanocapillary walls, as shown in Fig. 5. The directions in the image force are inward—pointing at each of the walls of the rhombus. For the rectangular capillary, the direction in the image force is codirectional with X and Y. The distances between the ion and each (C_1C_2, C_2C_3, C_3C_4, and C_4C_1) of the capillary inner surfaces are d_1, d_2, d_3, and d_4, as denoted in Fig. 5(b). The ion trajectories were calculated by solving Newton equations of motion in MATLAB [28]. The injection angles of the ions and the beam divergence are taken from the experiments. As seen in Fig. 4, the experimental transmission profiles for the capillaries of various cross sections are reproduced quite well by the simulations.

The image force increases with decreasing distance to the walls and corners; thus, ions entering close to the walls and corners of the rhombic or rectangular capillary hit the walls [see the image potential and particle trajectories in Figs. 5(a) and 5(b)]. For a given displacement of an ion from the center, the y component of the image force is larger than its x component [Fig. 5(b)], which results in a larger deflection by the image force along the short axes or sides than along the long axes or sides. Therefore, the transmitted angular distributions of the charged particles for the rhombic or rectangular capillaries are elongated more along the short axes or sides than along the long axes or sides [see Figs. 4(a) and 4(c)]. Our calculations follow the evolution of the flux distributions and the angular distributions of the ion beam along the capillary axis [26,27]. It is revealed from our calculations that the angular distribution of the ion beam possesses a circular shape at the entrance of the capillaries. In the capillary, the width first shrinks, then it becomes rhombic, and, around the middle of the capillary, it starts to expand due to defocusing caused by the image force. Close to the exit of the capillary, the charged particles with the largest deflection angles are blocked off, yielding the observed angular distributions [26]. Transmission occurs for all projectiles entering in a small region close to the center of the rhombus, while ions entering close to the corners and walls hit the walls, creating the observed angular distributions. This is revealed by the simulations of the ion trajectories in the case of rhombic capillaries [see Fig. 5(b)]. For the rhombic capillaries, the simulation yields ~0.8% transmission, quite close to the experimental value ~1.3%. In the case of rectangular capillaries, the simulated transmission rate and experimental values differ considerably (the experimental values are lower). The reason for this is presently not clear but may be due to size variations inside the channels; SEM studies of the phlogopite mica reveal that the channels may become narrower inside the membrane.

In conclusion, we investigated the influence of the shape of insulating nanocapillaries on the transmission profiles of keV Ne^{7+} ions, and our results clearly demonstrate that these profiles can be tailored by the geometrical cross sections of the nanocapillaries. We find that capillaries of rhombic cross sections produce rectangular shaped ion transmission profiles and, vice versa, that capillaries of rectangular geometry give a rhombic beam shape. This shaping effect only occurs for transmitted ions and is absent for the small fraction of ions that were neutralized. From simulations and the experimental findings, we derive that the shaping effect originates in the image forces seen by the ions in the walls of the nanocapillaries. We have investigated the effect for a large range of incident energies (7 keV up to 70 keV for Ne^{7+}) and for various ion charges and find that the shaping effect is thus rather universal [26]. The findings reveal a novel charged-particle beam shaping mechanism and suggest exploitation of capillaries of various conductivities and cross sections as a tool to guide and focus, as well as shape, ion beams for diverse applications.

We would like to thank the personnel of Stockholm University for the help with the ECR source and S-EBIT operation. We also thank Dr. Daniel Fischer, MPI, Heidelberg, for his assistance with the data acquisition system. This work was financially supported by the Knut & Alice Wallenberg Foundation, the European network ITS-LEIF, and by VR.

*Present address: School of Nuclear Science and Technology, Lanzhou University, Lanzhou 730000, China.
†Present address: School of Chemical Science and Engineering, Nuclear Chemistry, Royal Institute of Technology, SE-100 44 Stockholm, Sweden.
‡To whom correspondence should be addressed.
schuch@fysik.su.se

[1] C. R. Martin, Science **266**, 1961 (1994).
[2] S. E. Létant, T. W. van Buuren, and L. J. Terminello, Nano Lett. **4**, 1705 (2004).
[3] L. J. Steinbock, O. Otto, C. Chimerel, J. Gornall, and U. F. Keyser, Nano Lett. **10**, 2493 (2010).
[4] H. Daiguji, P. Yang, and A. Majumdar, Nano Lett. **4**, 137 (2004).
[5] S. Prakash, J. Yeom, N. Jin, I. Adesida, and M. A. Shannon, Proceedings of the Institution of Mechanical Engineers Part N, Journal of Nanoengineering and Nanosystems **220**, 45 (2006).
[6] M. Nishizawa, V. P. Menon, and C. R. Martin, Science **268**, 700 (1995).
[7] Z. S. Siwy, Adv. Funct. Mater. **16**, 735 (2006).
[8] M. Skupiński, A. Johansson, T. Jarmar, A. Razpet, K. Hjort, M. Boman, G. Possnert, and J. Jensen, Vacuum **82**, 359 (2007).
[9] T. Ikeda, Y. Kanai, T. M. Kojima, Y. Iwai, T. Kambara, Y. Yamazaki, M. Hoshino, T. Nebiki, and T. Narusawa, Appl. Phys. Lett. **89**, 163502 (2006).
[10] A. Cassimi *et al.*, Int. J. Nanotechnology **5**, 809 (2008).
[11] N. Stolterfoht, J.-H. Bremer, V. Hoffmann, R. Hellhammer, D. Fink, A. Petrov, and B. Sulik, Phys. Rev. Lett. **88**, 133201 (2002).
[12] D. S. Gemmell, Rev. Mod. Phys. **46**, 129 (1974).
[13] Gy. Víkor, R. T. Rajendra Kumar, Z. D. Pešic, N. Stolterfoht, and R. Schuch, Nucl. Instrum. Methods Phys. Res., Sect. B **233**, 218 (2005).
[14] Y. Kanai, M. Hoshino, T. Kambara, T. Ikeda, R. Hellhammer, N. Stolterfoht, and Y. Yamazaki, Phys. Rev. A **79**, 012711 (2009).
[15] N. Stolterfoht, R. Hellhammer, D. Fink, B. Sulik, Z. Juhász, E. Bodewits, H. M. Dang, and R. Hoekstra, Phys. Rev. A **79**, 022901 (2009).
[16] M. B. Sahana, P. Skog, Gy. Vikor, R. T. Rajendra Kumar, and R. Schuch, Phys. Rev. A **73**, 040901(R) (2006).
[17] P. Skog, H.-Q. Zhang, and R. Schuch, Phys. Rev. Lett. **101**, 223202 (2008).
[18] H.-Q. Zhang, P. Skog, and R. Schuch, Phys. Rev. A **82**, 052901 (2010).
[19] H. F. Krause, C. R. Vane, and F. W. Meyer, Phys. Rev. A **75**, 042901 (2007).
[20] P. Skog, I. L. Soroka, A. Johansson, and R. Schuch, Nucl. Instrum. Methods Phys. Res., Sect. B **258**, 145 (2007).
[21] Z. Juhász *et al.*, Nucl. Instrum. Methods Phys. Res., Sect. B **267**, 321 (2009).
[22] Y. Iwai, T. Ikeda, T. M. Kojima, Y. Yamazaki, K. Maeshima, N. Imamoto, T. Kobayashi, T. Nebiki, T. Narusawa, and G. P. Pokhil, Appl. Phys. Lett. **92**, 023509 (2008).
[23] K. Schiessl, W. Palfinger, K. Tőkési, H. Nowotny, C. Lemell, and J. Burgdörfer, Phys. Rev. A **72**, 062902 (2005).
[24] J. Ackermann, N. Angert, R. Neumann, C. Trautmann, M. Dischner, T. Hagen, and M. Sedlacek, Nucl. Instrum. Methods Phys. Res., Sect. B **107**, 181 (1996).
[25] S. R. Hashemi-Nezhad, Nucl. Instrum. Methods Phys. Res., Sect. B **234**, 533 (2005).
[26] H.-Q. Zhang *et al.* (unpublished).
[27] N. Akram *et al.* (unpublished).
[28] MATLAB version 6.5.2.202935, The MathWorks Inc., 2004.